Available online at www.sciencedirect.com

ScienceDirect

journal homepage: http://www.elsevier.com/locate/acme

Original Research Article

Texture, residual stresses and mechanical properties analysis in the commercial 1.4462 duplex stainless steel subjected to hydrostatic extrusion

Joanna Zdunek [a,*], *Piotr Maj* [a], *Mariusz Kulczyk* [b], *Jaroslaw Mizera* [a]

[a] *Warsaw University of Technology, Materials Science and Engineering Faculty, Woloska, 141, 02-507 Warsaw, Poland*

[b] *Institute of High Pressure Physics, Polish Academy of Sciences (Unipress), Warsaw, Poland*

ARTICLE INFO

Article history:
Received 11 July 2018
Accepted 14 December 2018
Available online 22 January 2019

Keywords:
Texture
Hydrostatic extrusion
Residual stresses

ABSTRACT

In the current research the hydrostatic extrusion (as one of the most common method of grain refinement) of the commercial 1.4462 duplex stainless steel was carried out using several reduction stages leading to a cumulative deformation strain $\varepsilon = 1.4$, and then $\varepsilon = 3.8$. The extrusion process has led to a change of microstructure and texture of the investigated material as was expected. Moreover, these changes were accompanied by improvements in mechanical properties measured by the nanohardness. The aim of this research was the characterization of the texture, residual stress and mechanical properties after subsequent stages of deformation.

1. Introduction

Duplex stainless steel (DSS) has many advantages over single – phase austenitic and ferritic alloys – among others high mechanical properties (e.g. tensile strength above 800 MPa and maximum elongation above 20%). Duplex stainless steels are about twice as strong as austenitic or ferritic stainless steels and have significantly better toughness and ductility than ferritic ones, however, they do not reach the excellent values of austenitic steels.

Furthermore corrosion resistance stands out – especially pitting and stress corrosion. Corrosion resistance depends mostly on the composition of the steel (especially content of the chromium and molybdenum is important), but duplex stainless steel grades have a range of corrosion resistance, similar to the range for austenitic stainless steels. DSS show also very good stress corrosion cracking resistance, a property they have gained from the ferritic phase. In addition, the physical and mechanical properties of DSS, may vary depending on the temperature, the size and shape of the grains of both phases, the surface area of the interphase boundaries and the precipitation of intermetallic phases.

The best composition of properties can be obtained by a phase composition of about 50% ferrite and 50% austenite. This can be controlled by chemical composition and proces-

* *Corresponding author.*
E-mail address: joanna.zdunek@pw.edu.pl (J. Zdunek).

https://doi.org/10.1016/j.acme.2018.12.008
1644-9665/

sing conditions. The typical DSS microstructure consists of austenite islands in a ferritic matrix [1].

Due to the lower alloying content, duplex stainless steels can be lower in cost – DSS have lower nickel and molybdenum contents than the austenitic grades of similar corrosion resistance. Additionally, due to the potentiality of the reduction of the section thickness due to increased yield strength of DSS compared to austenitic stainless steel there is a possibility to lower the costs of production. This can lead to cost and weight savings compared to products made of austenitic stainless steels.

However, DSS has also some disadvantages – among others the most important is its moderate formability and machinability. Additionally, at increased temperature (above 300 °C) or during slow cooling after annealing, a tendency was observed for the formation of brittle σ, Cr_2N, Π phases, which may also affect the reduction of corrosion resistance and ductility [2]. As mentioned before, the two-phase structure provides the increased strength and hardness and further these properties, providing duplex stainless steel with high resistance to erosion and wear. Other physical property described in this category is steel linear expansion coefficient that is much lower than that for austenitic steels. This coefficient is rather close to the coefficient for carbon steel, which is especially important when welding different types of steel in a particular construction.

Since the pioneering work of Hall and Petch, scientists and engineers are interested in materials with small grain sizes. According to Hall–Petch dependence, a smaller grain size increases the strength and the fracture toughness of the material. Traditional thermo-mechanical processes can lead to a grain size above 10 μm or, exceptionally, a few microns in diameter [3]. Hence there was a necessity to develop techniques enabling to obtain submicron or nano-sized grains. Severe plastic deformation (SPD) belongs to the top-down approach and describes a group of methods used for producing ultrafine-grained and nanocrystalline materials [4]. The most common methods in the SPD group are: equal channel angular pressing (ECAP) or equal channel angular extrusion (ECAE) [5,6], high-pressure torsion (HPT) [7,8], accumulated roll bonding (ARB) [9], cyclic extrusion–compression (CEC) [10], etc. A comprehensive study together with the list of contemporary methods included in the SPD can be found in Diamond Jubilee issue of Acta Materialia [11]. One of the popular methods leading to grain refinement, but not included in SPD method (according to well known definition which can be found e.g. in [11]) is hydrostatic extrusion (HE) [12,13]. The idea of this method is to induce high strains during forming using a liquid medium to avoid friction between stamp and material. To achieve that, the work piece is held in sealed chamber surrounded by pressurized liquid (the force is delivered through the piston/stamp) and therefore liquid applies pressure to all surfaces of extruded material. Due to large deformation the microstructure undergoes a series of transformations. Grain refinement at high strains implies the creation of new high angle grain boundaries which can be accomplished by three mechanisms [14]. The first is the elongation of existing grains during plastic deformation, causing an increase in high angle boundary area. The second is the creation of high angle boundaries by grain subdivision mechanisms. Finally an elongated grain can be split up by a localization phenomenon such as a shear band. The second mechanism is considered probably the most important. After the process, the material exhibits increased strength and reduced elongation which is due to the decrease of the dislocation mobility.

Various materials can react differently to SPD processes and the details of the grain refinement process are not fully understood yet [15].

In case of two-phase alloys, there are more opportunities of treatment to form the structure by combining the process of plastic deformation with recrystallization and precipitation processes [16]. Moreover, DSS is characterized by the presence of two types of internal borders, namely grain boundaries and interphase boundaries. The presence of interphase boundaries has a significant impact both on the process of plastic deformation and recrystallization [17].

In the DSS, due to high strain, the transformation of the austenite takes place and as a result deformation induced ferrite α' is created (particular in the stress concentration sites). The results indicate that after SPD the material may undergo microstructural changes induced by plastic deformation [18–20]. During deformation the material gains additional energy resulting from imposed strain. An excessive amount of dislocation is generated and lattice parameters change their values slightly. These conditions favor thermodynamically stable phases whereas metastable have decreased activation energy especially in locally strained regions. The above description applies particularly to TRIP steels although austenitic and DSS steels may also be affected [18,21,22]. It is known that low stacking fault energy (SFE) facilitates $\gamma \rightarrow \alpha'$ transformation [23]. The $\gamma \rightarrow \alpha'$ transformation was observed by the authors in their previous work [24] concerning the DSS and widely described. The results obtained by means of XRD and TEM observation clearly indicate that the transformation did occur in a 1.4462 duplex steel after the last stage of deformation.

Another important aspect in the study of duplex steels is the residual stress. Residual stresses can be defined as the stresses which remain in a material in the absence of any external forces. There are many stress determination methods – destructive and nondestructive and X-ray residual stress measurement is considered as a nondestructive method. This method uses the distance between crystallographic planes d as a strain gauge. The deformations cause changes in the d spacing of the lattice planes from their stress free value to a new value that corresponds to the magnitude of the residual stress. The method used in the experimental calls $\sin^2\Psi$ and has involved determination of d spacing as a function of $\sin^2\Psi$ where Ψ is a tilt angle. In the current research the authors want to revise the current viewpoint on the texture, residual stresses and mechanical properties changes in duplex steel after hydrostatic extrusion. The paper is a continuation of the previous article concerning this topic entitled ''Microstructure and mechanical properties of duplex stainless steel subjected to hydrostatic extrusion'' [24]. The current analysis is focused on the differences in deformation of austenite and ferrite due to their different properties coming from crystallographic structure. The results have shown that

the response of both phases is different and varies with cumulative strain.

2. Material and experimental procedures

The investigated duplex stainless steel was a commercial 1.4462 duplex stainless steel with the chemical composition (wt.%) as given in Table 1.

The initial billet with a diameter of 20 mm was extruded at room temperature in eight consecutive steps. Fig. 1 presents the scheme of the diameter reduction. The process was performed at the Institute of High Pressure Physics "UNIPRESS" (Poland) – details were given in previous published paper [24].

Texture analysis was performed using a Bruker D8 Discover diffractometer equipped with a Cr anode (wavelength $K_{\alpha 1}$ $\lambda = 2.29$ Å) with collimated point beam of approximately 1 mm diameter. The measurements were conducted on the cross section cut from the billet center at the initial state and after HE with deformation $\varepsilon = 1.4$ and $\varepsilon = 3.8$. During the experiment the incomplete pole figures (PFs) were obtained on the most intensive crystallographic planes (first three) of austenite: {1 1 1}, {2 0 0}, {2 2 0} and ferrite {1 1 0}, {2 0 0}, {2 2 1} for each deformation value, from which orientations distribution functions (ODFs) in Bunge's notation (φ_1, ϕ, φ_2) were calculated using the spherical harmonics method (ODFs in Figs. 2–4 are presented for φ_2 const.).

The residual stresses were measured using $\sin^2\Psi$ X-ray diffraction method. The advantage of the used diffraction method is the possibility to gain information about two phases discretely. The diffraction angle 2Θ, was measured experimentally and then the lattice spacing d was calculated from the diffraction angle of (2 2 0) plane for austenite and (2 1 1) for ferrite. The interplanar spacing $d_{h\,k\,l}$ was determined using Bragg's law from the diffraction peak, which was obtained by fitting a Gaussian function to the diffraction profile. The $d_{h\,k\,l}$–spacing values were plotted vs. $\sin^2\Psi$, where Ψ is the tilt angle varying from 0 to 60°.

Nanohardness measurements were carried out using the Hysitron Triboindenter TI950 nanotester which is a very precise, fully automated research instrument for characterizing materials on a nanometric scale. The multilayer housing and the active anti-vibration insulation system integrated with the heads and electronics ensure separation of the tested sample from the ambient conditions. A Berkovich indenter (diamond trigonid) was used. The stiffness parameters of the indenter are: $E = 1140$ GPa, $\nu = 0.07$. The maximum load during the test was 2 mN, loading time and unloading time 10 s, and the holding time at the maximum load of 2 s.

3. Results

The initial study of the investigated material concerned the characterization of the microstructure and the detailed description of those results was presented in Ref. [24]. The present study has focused on the texture and residual stresses evolution caused by the high strains induced by the hydrostatic extrusion.

3.1. *Texture*

The obtained texture results for the initial state are presented as an Orientation Distribution Function (ODF) in Fig. 2. This figure shows that ODFs for austenite (a) and ferrite (b) have revealed the presence of a texture at the initial state, wherein the austenite texture is less pronounced than the ferrite one (the maximum value for austenite is 20.26, and 149.30 for ferrite). In case of ferrite the peak is also less diffused compared to austenite. The main texture component for the austenite was identified as *rotated cube* {0 0 1} ⟨1 1 0⟩ (but deviates 5° from ideal position) and for ferrite the main is so called *cube* component {1 0 0} ⟨0 0 1⟩ (also deviates 5° from ideal position). The cube component was reported in the literature for different duplex steels as a recrystallization texture component [25]. The authors of [25] have stated that it is a one of the most stable components during plane strain compression e.g. rolling [26,27]. Quantitative analysis of the texture components indicate that austenite is in 28% *rotated cube* and ferrite is in 44% *cube* in the investigated material. The rest of orientations are random ones. Table 2 contains volume fractions of particular texture components calculated by Model Function Method in Labo Tex 3.0 software.

The initial materials were then subjected to hydrostatic extrusion and at the first investigated state $\varepsilon = 1.4$ (rods

Table 1 – The chemical composition of 1.4462 duplex steel [wt.%].

	Cr	Ni	Mo	Mn	C	N	Fe
wt.%	21–23	4.5–6.5	2.5–3.5	Max 2	Max 0.3	0.02–0.08	Balance

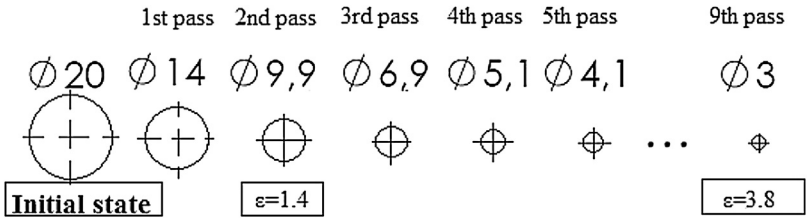

Fig. 1 – Scheme of the diameter reduction during the hydrostatic extrusion.

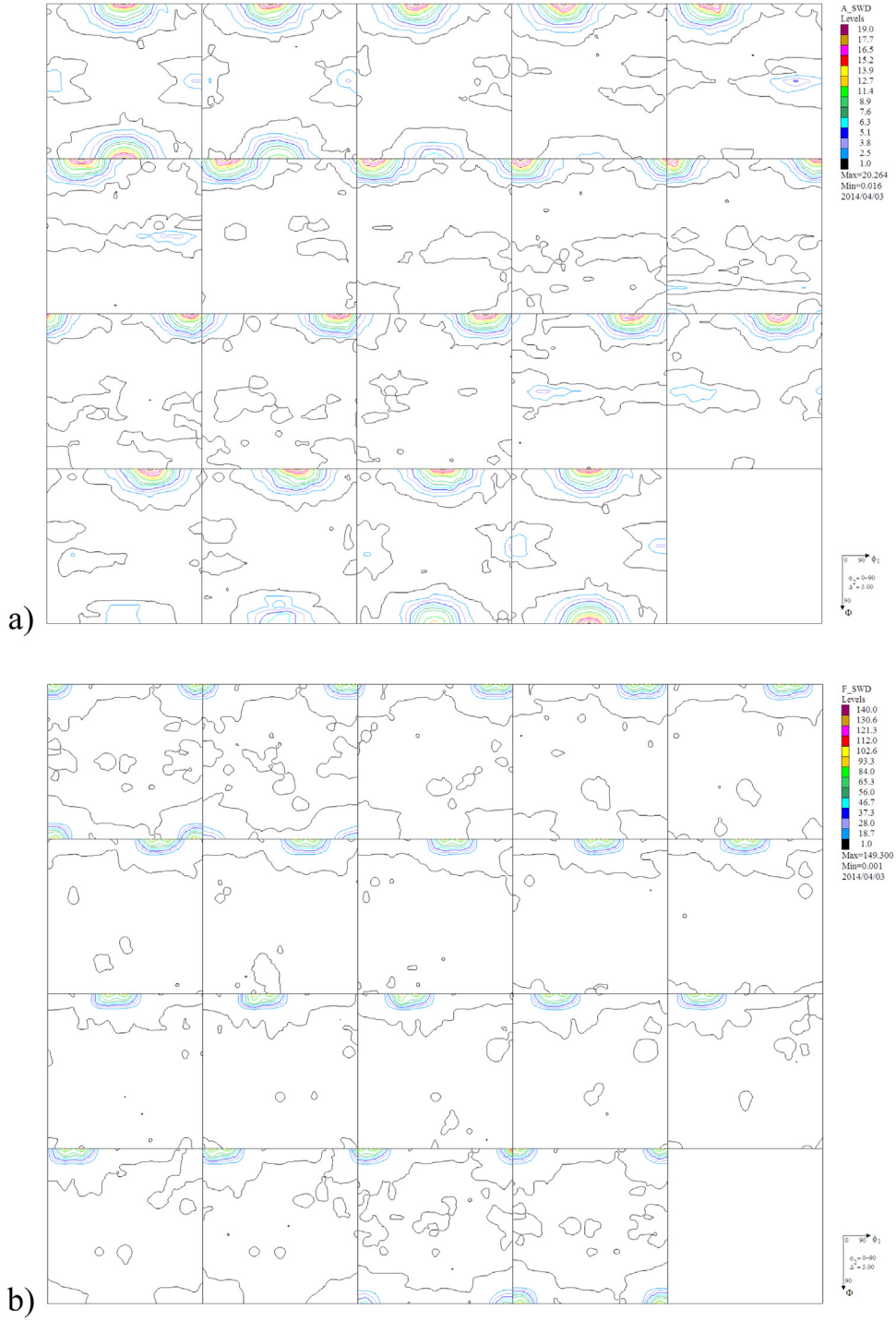

Fig. 2 – Orientation distribution functions for austenite (a) and ferrite (b) at the initial state.

diameter reduction from 20 to 5 mm) the ODFs have shown typical for extruded materials strong axial texture with main fiber component γ ⟨1 1 1⟩ and ⟨0 0 1⟩ type for austenite and for ferrite there are two ''rolling texture'' components (0 7 1 0) ⟨1 0 0⟩ (34%) and (0 7 1 0) ⟨0107⟩ (32%) and ⟨1 1 3⟩ fiber (4%). These two rolling type components are close to ⟨1 1 0⟩ fiber and at the 3D Euler space diagram looks like split fiber. In the austenite there is also some presence of the *rotated cube* component as a residue from the initial state. Quantitative analysis of the texture components indicate that austenite is in 38% ⟨1 1 1⟩ fiber, 31% ⟨0 0 1⟩ and 6% *rotated cube*. It is worth to mention that ferrite has occurred to be much more textured

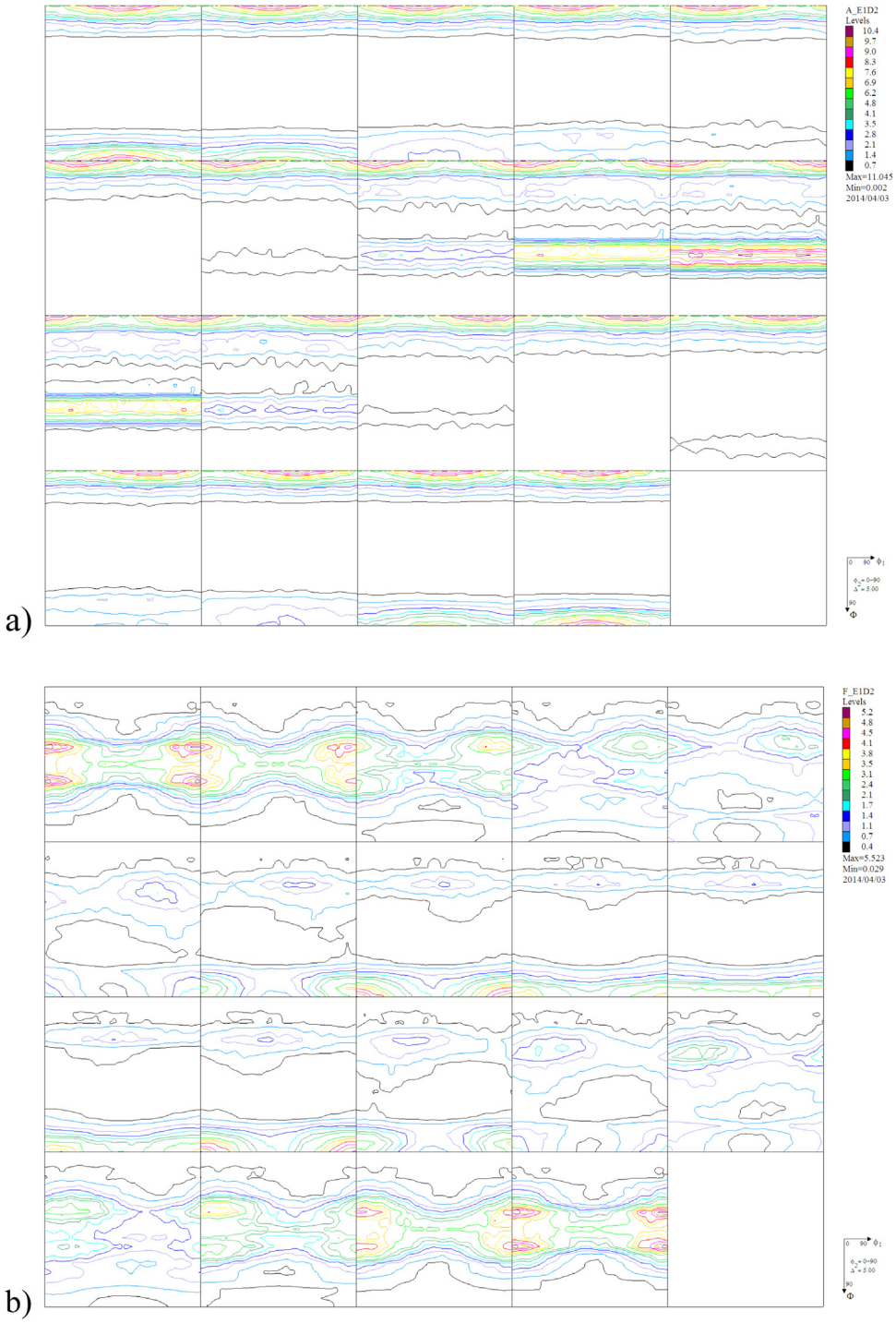

Fig. 3 – Orientation distribution function for austenite (a) and ferrite (b) after HE $\varepsilon = 1.4$.

than austenite – just like at the initial state. Fig. 3 shows ODFs for austenite (a) and ferrite (b). Additionally the ⟨1 1 0⟩ fiber in ferrite is visibly split (or blurry).

After the next step of deformation obtained by HE (cumulative deformation value $\varepsilon = 3.8$) the character of the texture has noticeably changed. Although, the axial texture is still present, the fiber component is significantly fragmented and/or blurry, which is illustrated in the ODFs (Fig. 4a and b) for both phases. Both ferrite and austenite ODFs have revealed that the fibers changed to incomplete/fragmented fibers, but despite this texture is still noticeable. There is some literature indicating that the ⟨1 1 1⟩ texture component is much more stable during the deformation of the FCC polycrystal, e.g. [28], and the presence of this component with the increased deformation value in the investigated material was also expected. In this case the austenite revealed that ⟨1 1 1⟩ fiber

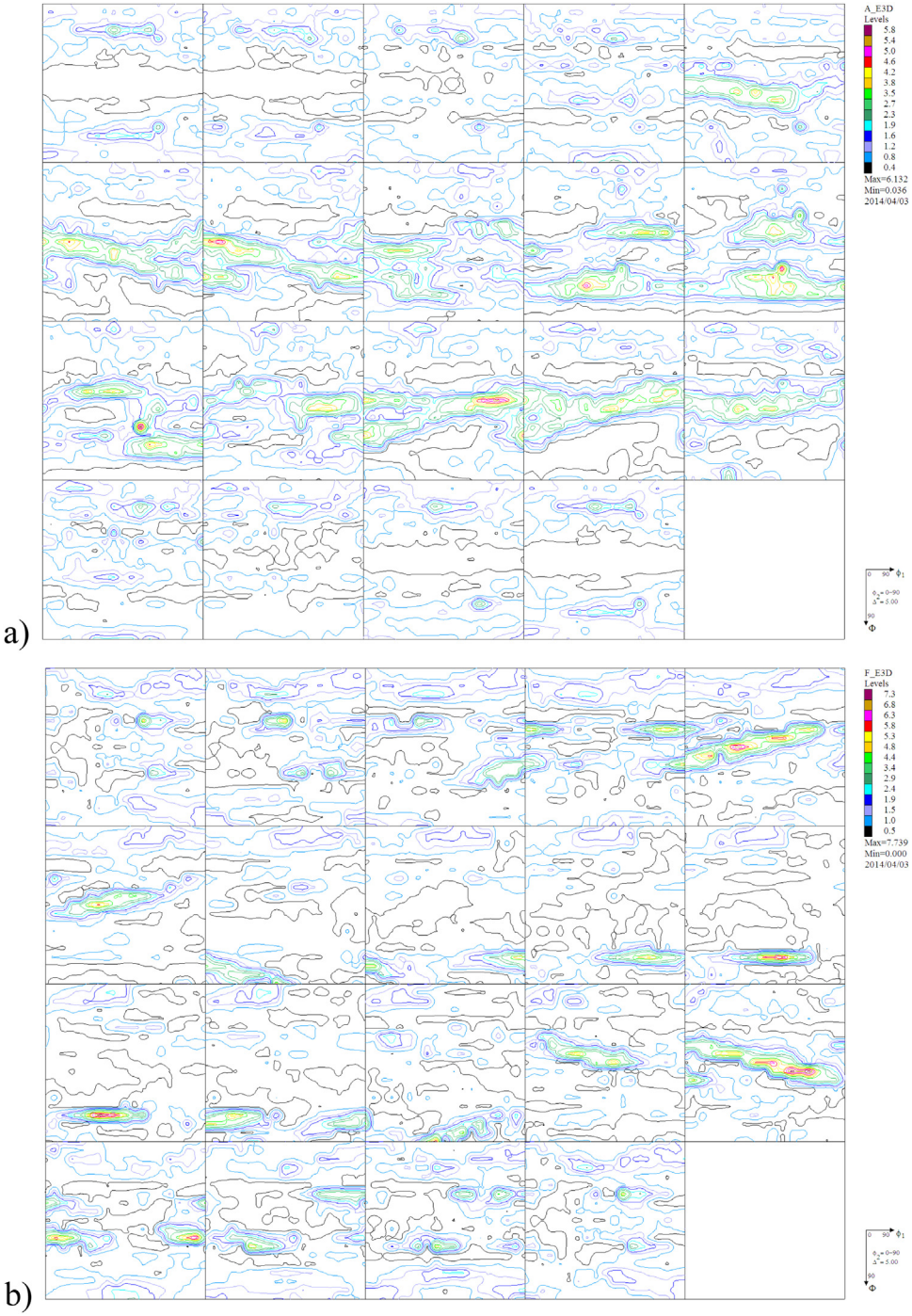

Fig. 4 – Orientation distribution function for austenite (a) and ferrite (b) after HE $\varepsilon = 3.8$.

texture component is missing and its place took few fibers close to the ⟨2 2 1⟩ orientation in 16%. For the ferrite fiber close to ⟨8 8 3⟩ appeared in 21%.

In all the investigated cases (initial state, after HE with $\varepsilon = 1.4$ and $\varepsilon = 3.8$) the ferrite texture was more developed (stronger) and had higher intensities than the austenite texture. Similar observations were made by C. Herrera et al. [26]. They have examined microstructure and texture of hot-rolled duplex stainless steel and also had noticed that ferrite has a more intensive texture that austenite after deformation. In their case the intensity has increased with deformation. Comparing the results for the hot rolled and extruded duplex steel one can detect similarities in the texture components – especially at the initial state. In both (rolled and extruded) phases *cube* {0 0 1} ⟨1 0 0⟩ for ferrite and *rotated cube* {1 0 0} ⟨0 1 1⟩ for austenite is present. Herrera et al. have reported that

Table 2 – Main texture components in austenite and ferrite phase at all investigated states.

	Austenite	Volume [%]	Ferrite	Volume [%]
Initial state	*Rotated cube* {1 0 0} ⟨0 1 1⟩	28	*Cube* {1 0 0} ⟨0 0 1⟩	44
$\varepsilon = 1.4$	γ ⟨1 1 1⟩	38	⟨1 1 3⟩	γ ⟨1 1 1⟩
	⟨0 0 1⟩	31	(0 7 1 0) ⟨1 0 0⟩	34
	{1 0 0} ⟨011⟩	6	(0 7 10) ⟨0107⟩	32
$\varepsilon = 3.8$	⟨221⟩	16	⟨8 8 3⟩	21

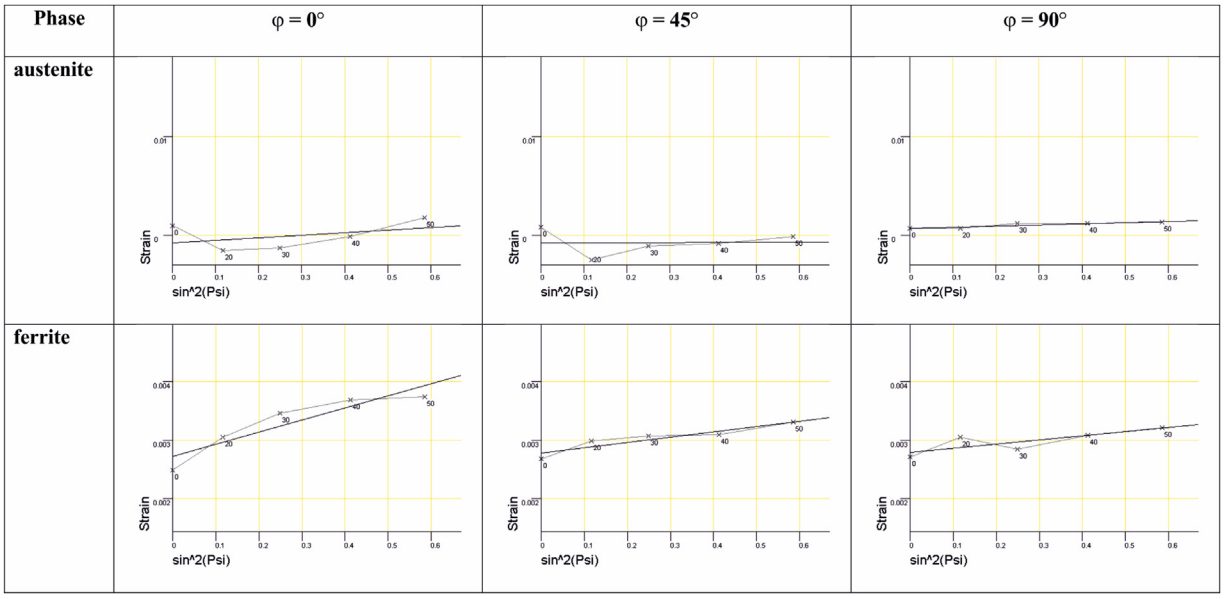

Fig. 5 – Plots $d_{h\,k\,l}$ ($\sin^2\psi$) for austenite (a) and ferrite (b).

according to Raabe et al. [29] the rotated cube, {1 0 0} ⟨0 1 1⟩, tends to undergo recovery rather than recrystallization due to its small in – grain orientation gradients.

3.2. *Residual stress*

A diffractometer with Cr radiation was used to measure the interplanar spacing of the {2 1 1} planes in the ferritic phase and of the {2 2 0} planes in the austenitic phase. As was mentioned before, $\sin^2\psi$ method was used to determine residual stresses. Plots $d_{h\,k\,l}$ vs. $\sin^2\psi$ are presented in Fig. 5. In order to make three-dimensional stress analysis possible, lattice displacements were determined in 3φ – directions (0°, 45°and 90°) for 11 ψ-angles between 0 and 60° for both phases. The locations of the diffracted peaks were determined by a least squares fit of a pseudo-Voigt function to the data. The unstressed lattice parameters *a* for each phase in the investigated material were determined previously to be 3.59694 ± 0.00020 Å for austenite and 2.87355 ± 0.00018 Å for ferrite [26]. The stress tensor was determined in each phase by a least-squares procedure. Table 3 contains a normal stress values in three directions (0, 45 and 90°) and main stress values σ_1 and σ_2 calculated from the tensor. The obtained values indicate that internal residual stress increased after being subjected to plastic deformation. In all cases stresses were not isotropic – one can notice tensile and compression stress σ_1 and σ_2 in Table 3 (only the initial state can be considered isotropic in terms of stress distribution in three directions). This can be connected with the strong texture in the investigated material which influences on the measured interplanar spacing. Dakhlaoui et al. [30] reported that anisotropic behavior of polycrystalline grains can be predicted by using anisotropy of single elastic constants and crystallographic texture as a part of experiment.

Table 3 – Normal and main stresses values for austenite and ferrite at initial state and after HE $\varepsilon = 1.4$ and $\varepsilon = 3.8$.

	Normal stresses [MPa]			Main stresses	
	σ_{0°	σ_{45°	σ_{90°	σ_1	σ_2
Austenite initial	121 ± 11	137 ± 16	129 ± 13	356	97
Austenite $\varepsilon = 1.4$	420 ± 24	23 ± 8	190 ± 16	754	−61
Austenite $\varepsilon = 3.8$	537 ± 17	-95 ± 22	431 ± 28	1035	−81
Ferrite initial	-89 ± 27	-108 ± 31	-97 ± 22	169	20
Ferrite $\varepsilon = 1.4$	110 ± 16	-124 ± 21	-53 ± 13	220	−158
Ferrite $\varepsilon = 3.8$	621 ± 51	269 ± 33	446 ± 56	790	267

Table 4 – Nano hardness of the material at the initial state and after HE $\varepsilon = 1.4$ and $\varepsilon = 3.8$.

	Nano-hardness [GPa]	Standard deviation [GPa]	Spread of results [GPa]
Initial state	4.18	0.24	1.13
$\varepsilon = 1.4$	5.03	0.38	1.65
$\varepsilon = 3.8$	5.59	0.48	2.15

3.3. *Nanohardness tests*

The aim of the test was to analyze the properties on the sub–micron level and to investigate the homogeneity of the duplex steel after subsequent stages of deformation. The results obtained have proved that after $\varepsilon = 3.8$ the material has the highest hardness among all the tested materials (see Table 4). They also indicate that the mechanical properties may vary significantly depending on the measurement points. This heterogeneity was also examined previously [24] using transmission microscopy. The measurements were done in 50 μm intervals in the x and y-axis, overall 25 measurements. Due to strong refinement and deformation it was hard to distinguish the precise values of individual phases. During the measurement, however, it was noticeable that austenite rich regions had higher values of hardness (up to 6 GPa), whereas ferrite regions had a value of 4.3 GPa. Large differences in values and number of results exclude measurement error.

4. Discussion

The current research concerns the analysis of differences in austenite and ferrite deformation in DSS subjected to hydrostatic extrusion which in general lead to the improvement of the mechanical properties determined in the test of nano-hardness. It has been shown that the reaction on the imposed stress in ferrite and austenite differs significantly. This is apparent when analyzing simultaneously the results of microstructure, texture, and residual stresses and nano-hardness. The observed differences are a result of distinctive crystallographic structures. Austenite and ferrite have respectively FCC and BCC primitive cells with different plastic deformation slip planes. Different responses of both phases are further driven by SFE 700 mJ/m^2 [31] and 15 mJ/m^2 [32] respectively for ferrite and austenite. After the first stage of deformation only typical extrusion slip planes are activated ($\langle 1\,1\,1\rangle$ and $\langle 1\,1\,0\rangle$ respectively for austenite and ferrite). Further deformations leads to activation of other slip planes that causes further distortion of crystal lattice and grain refinement (previous investigations have indicated that it was especially in the ferrite region). Furthermore as a result of imposed strain $\gamma \rightarrow \alpha'$ transformation takes place in the material [24]. It is possible that further deformations cause further tension between interphase boundaries. Gamma transformations are more favorable from the viewpoint of thermodynamic system.

Texture results confirm that both phases behave differently when stress is imposed in the material. In the case of first stage of deformation preferential slip systems for extrusion are seen both in austenite and ferrite respectively $\langle 0\,0\,1\rangle$ and $\langle 1\,1\,0\rangle$. The texture sharpness increase with deformation range from $f_2 = 1.97$ to $f_2 = 4.81$ for ferrite and from $f_2 = 3.94$ to $f_2 = 4.11$ for austenite. At the final stage of deformation ($\varepsilon = 3.8$) a rapid change of texture has occured in the material. As a result the α fiber becomes blurry and fragmented in the Euler space. This is a result of $\gamma \rightarrow \alpha'$ transformation and increasing of the refinement of the structure.

Equally important are the results of normal and main stresses values. Both phases display relatively low shear strain after subsequent stages of deformation compared to equal channel angular pressing [33]. Furthermore the largest stress is present along the extrusion direction σ_0 slightly lower values are present in perpendicular direction. This is due to the reduction of the cross section of the sample. Comparing the effective cumulative strain it can be seen that austenite has a high base line of stress compared to ferrite with $\varepsilon = 1.4$. However for the highest level of deformation this changes in favor to ferrite. This proves that in the early stages of deformation the stress is mainly transferred by austenite but later during the process it stops at a certain level whereas in ferrite the ability to undergo plastic deformation is much higher. This effect increases together with the degree of $\gamma \rightarrow \alpha'$ transformation leads to a more efficient strengthening of the material compared to austenite or ferrite single phase steels [34].

The conducted nanoindentation tests allowed the characterization of the mechanical properties in the sub-micron scale. The tests were necessary to describe the changes that occur in the material after subsequent stages deformation. On their basis homogeneity of the material was determined. The spread and standard deviation rose with cumulative strain. The difference between individual values is mostly a result of unequal responses to strain during deformation for ferrite and austenite. For the highest observed strain it is over 2 GPa. However it must be noted that the intender area covered both ferrite and austenite nonetheless their volume fraction was uneven due to the small point measurement.

The obtained data has indicated that value and direction of residual stresses (compressive or tensile) are related to initial texture of the material. The induced strains (by hydrostatic extrusion) have caused texture-related anisotropy. Position of the stress tensor relative to the main components forming the texture generates different density of dislocations and activates various slip systems (also in close relation to the crystal lattice of the material – FCC or BCC). It also affects the defect arranging in the deformed material and hence the differences in mechanical properties.

The issue of heterogeneous deformation in duplex steel has been described in a variety of scientific studies [35–38]. It seems obvious that ferrite and austenite behave differently when deformation is introduced into the material. This effect is evident on many levels starting with texture through microstructure and mechanical properties. Based on the current results and the available literature [39] it can be concluded that the changes are more rapid in austenite in

the early stages of deformation later they stabilize [18]. On the other ferrite undergoes constant changes. This is most apparent when comparing residual stresses in particular stages of deformation.

5. Conclusions

The paper describes the changes of texture, residual stress, microstructure and nanohardness after hydrostatic extrusion process. From the current work the following conclusions can be drawn:

The change rate in austenite is greater, although after the early stages of deformation a stabilization occurs in the material. The changes in ferrite are more gradual through individual stages of deformation.

As a result of extrusion a change in texture can be observed in the tested duplex steel. Starting from recrystallization texture to a typical extrusion texture along slip planes ⟨1 1 0⟩ and ⟨1 1 1⟩, respectively for ferrite and austenite. After the last stage of deformation the determination of texture is no longer so simple/obvious. In this case lattice distortion and $\gamma \rightarrow \alpha'$ plays an important role.

The microstructure inhomogeneity is followed by the mechanical properties improvement. Generally the hardness rises with cumulative strain although the difference become significant reaching a spread of 2 GPa.

Acknowledgements

Financial support of the European Regional Development Fund through the Structural Funds in the Operational Program – Innovative Economy (IE OP) – Project No. POIG.01.03.01-00-015/08 (NANOMET) is gratefully acknowledged.

REFERENCES

[1] M.R. Miranda, J.M. Sasaki, S.S.M. Tavares, H.F.G. De Abreu, J. M. Neto, The use of X-ray diffraction, microscopy, and magnetic measurements for analysing microstructural features of a duplex stainless steel, Mater. Charact. 54 (2005) 387–393.
[2] J.C. Lippold, D. Kotecki, Welding Metallurgy and Weldability of Stainless Steel, John Wiley & Sons, New Jersey, 2005.
[3] Verlinden B, Severe plastic deformation of metals, Association of Metallurgical Engineers Serbia and Montenegro Scientific paper AME DC:669.01:620.174/.175=20 MJOM Metalurgija - Journal of Metallurgy, 165-182.
[4] R.Z. Valiev, R.K. Islamgaliev, I.V. Alexandrov, Bulk nanostructured materials from severe plastic deformation, Prog. Mater. Sci. 45 (2000) 103–189.
[5] Y.T. Zhu, T.C. Lowe, Observations and issues on mechanisms of grain refinement during ECAP process, Mater. Sci. Eng. A 291 (2000) 46–53.
[6] Y.H. Zhao, X.Z. Liao, Z. Jin, R.Z. Valiev, Y.T. Zhu, Microstructures and mechanical properties of ultrafine grained 7075 Al alloy processed by ECAP and their evolutions during annealing, Acta Mater. 52 (2004) 4589–4599.
[7] A. Vorhauer, R. Pippan, On the homogeneity of deformation by high pressure torsion, Scr. Mater. 51 (2004) 921–925.
[8] G. Sakai, K. Nakamura, Z. Horita, T.G. Langdon, Developing high-pressure torsion for use with bulk samples, Mater. Sci. Eng. A 406 (2005) 268–273.
[9] Y. Saito, N. Tsuji, H. Utsunomiya, T. Sakai, R.G. Hong, Ultra-fine grained bulk aluminum produced by accumulative roll-bonding (ARB) process, Scripta Mater. 39 (1998) 1221–1227.
[10] Y.J. Chen, Q.D. Wang, H.J. Roven, M.P. Liu, M. Karlsen, Y.D. Yu, J. Hjelen, Network-shaped fine-grained microstructure and high ductility of magnesium alloy fabricated by cyclic extrusion compression, Scripta Mater. 58 (2008) 311–314.
[11] Y. Estrin, A. Vinogradov, Extreme grain refinement by severe plastic deformation; a wealth of challenging science, Acta Mater. 61 (2013) 782–817.
[12] B. Adamczyk-Cieślak, J. Mizera, K.J. Kurzydłowski, Microstructures in the 6060 aluminium alloy after various severe plastic deformation treatments, Mater. Charact. 62 (2011) 327–332.
[13] J. Bohlen, S.B. Yi, J. Swiostek, D. Letzig, H.G. Brokmeier, K.U. Kainer, Microstructure and texture development during hydrostatic extrusion of magnesium alloy AZ31, Scr. Mater. 53 (2005) 259–264.
[14] J. Gill Sevillano, P. Van Houtte, E. Aernoudt, Prog. Mater. Sci. 25 (1980) 69–412.
[15] Y. Estrin, A. Vinogradov, Extreme grain refinement by severe plastic deformation: a wealth of challenging science, Acta Mater. 61 (2013) 782–817.
[16] J. Ryś, A. Zielińska-Lipiec, Structural aspects of ferrite and austenite co-deformation in duplex stainless steel, Solid State Phenom. 203–204 (2013) 28–33.
[17] M. Liljas, P. Johansson, H.P. Liu, C.O.A. Olsson, Development of a lean duplex stainless steel, Steel Res. Int. 79 (2008) 466–473.
[18] A. Belyakov, Y. Kimura, K. Tsuzaki, Microstructure evolution in dual-phase stainless steel during severe deformation, Acta Mater. 54 (2006) 2521–2532.
[19] S.S.M. Tavares, M.R. da Silva, J.M. Pardal, H.F.G. Abreu, A.A. Gomes, Microstructural changes produced by plastic deformation in the UNS S31803 duplex stainless steel, J. Mater. Process Technol. 180 (2006) 318–322.
[20] E.S. Perdahcioglu, H.J.M. Geijselaers, J. Huétink, Influence of stress state and strain path on deformation induced martensitic transformations, Mater. Sci. Eng. A 481–482 (2008) 727–731.
[21] S.S.M. Tavares, D. Gunderov, V. Stolyarov, J.M. Neto, Phase transformation induced by severe plastic deformation in the AISI 304L stainless steel, Mater. Sci. Eng. A 358 (2003) 32–36.
[22] L. Chen, F.P. Yuan, P. Jiang, X.L. Wu, Mechanical properties and nanostructures in a duplex stainless steel subjected to equal channel angular pressing, Mater. Sci. Eng. A 551 (2012) 154–159.
[23] S. Allain, J.-P. Chateau, O. Bouaziz, S. Migot, N. Guelton, Correlations between the calculated stacking fault energy and the plasticity mechanisms in Fe–Mn–C alloys, Mater. Sci. Eng. A 387–389 (2004) 158–162.
[24] P. Maj, B. Adamczyk-Cieślak, J. Mizera, W. Pachla, K.J. Kurzydłowski, Microstructure and mechanical properties of duplex stainless steel subjected to hydrostatic extrusion, Mater. Charact. 93 (2014) 110–118.
[25] D. Raabe, Texture and microstructure evolution during cold rolling of a strip cast and of a hot rolled austenitic stainless steel, Acta Mater. 45 (1997) 1137–1151.
[26] C. Herrera, D. Ponge, D. Raabe, Microstructure and texture of hot-rolled duplex stainless steel, in: 3rd Int. Conf. Thermomechanical Process. Steels, TMP, vol. 2008, 2008.
[27] F.J. Humphreys, M. Hatherly, Recrystallization and Related Annealing Phenomena, Elsevier, 2004.

[28] D. Jakubowska, J. Zdunek, M. Kulczyk, J. Mizera, K.J. Kurzydłowski, Microstructure and texture of hydrostatic extrusion deformed ni single crystals and polycrystal, Adv. Mater. Sci. Eng. (2015) 1–7.
[29] D. Raabe, Overview on basic types of hot rolling textures of steels, Steel Res. 74 (2003) 327–337.
[30] R. Dakhlaoui, A. Baczmański, C. Braham, S. Wroński, K. Wierzbanowski, E.C. Oliver, Effect of residual stresses on individual phase mechanical properties of austeno-ferritic duplex stainless steel, Acta Mater. 54 (2006) 5027–5039.
[31] W. Reick, M. Pohl, A.F. Padilha, Fe–Cr–Ni (DIN 1.4462): stacking faults, Steel Res. 67 (1996) A364.
[32] A. Machov, G.E. Beltz, M. Chang, Atomistic simulation of stacking fault formation in bcc iron, Modell. Simul. Mater. Sci. Eng. 7 (1999) 949–974.
[33] J. De Messemaeker, B. Verlinden, J. Van Humbeeck, Texture of if steel after equal channel angular pressing (ECAP), Acta Mater. 53 (2005) 4245–4257.
[34] B. Kim, T.T.T. Trang, N.J. Kim, Deformation behavior of ferrite-austenite duplex high nitrogen steel, Met. Mater. Int. 20 (2014) 35–39.
[35] R.L. Peng, J. Gibmeier, G.C. Chai, S. Johansson, Load partitioning in a duplex stainless steel with surface strength gradient and residual stresses, Adv. X-Ray Anal. (2008) 773–780.
[36] C.H. Seo, K.H. Kwon, K. Choi, K.H. Kim, J.H. Kwak, S. Lee, et al., Deformation behavior of ferrite-austenite duplex lightweight Fe–Mn–Al–C steel, Scr. Mater. 66 (2012) 519–522.
[37] W. Zieliński, W. Świątnicki, M. Barstch, U. Messerschmidt, Non-uniform distribution of plastic strain in duplex steel during TEM in situ deformation, Mater. Chem. Phys. 81 (2003) 476–479.
[38] N. Jia, R. Lin Peng, Y.D. Wang, S. Johansson, P.K. Liaw, Micromechanical behavior and texture evolution of duplex stainless steel studied by neutron diffraction and self-consistent modeling, Acta Mater. 56 (2008) 782–793.
[39] Y. Cao, Y.B. Wang, X.H. An, X.Z. Liao, M. Kawasaki, S.P. Ringer, et al., Concurrent microstructural evolution of ferrite and austenite in a duplex stainless steel processed by high-pressure torsion, Acta Mater. 63 (2014) 16–29.